Perovskite/Polymer Monolithic Hybrid Tandem Solar Cell Utilizing Low-temperature, Full Solution Process

Journal:	*Materials Horizons*
Manuscript ID:	MH-COM-12-2014-000237.R1
Article Type:	Communication
Date Submitted by the Author:	03-Jan-2015

Complete List of Authors:	Chen, Chun-Chao; University of California, Department of Materials Science and Engineering Bae, Sang-Hoon; University of California, Department of Materials Science and Engineering Chang, Wei-Hsuan; University of California, Department of Materials Science and Engineering Hong, Ziruo; University of California, Department of Materials Science and Engineering Li, Gang; University of California, Department of Materials Science and Engineering Chen, Qi; University of California, Los Angeles, Materials Science and Engineering Zhou, Huan-Ping; University of California, Department of Materials Science and Engineering Yang, Yang; University of California, Department of Materials Science and Engineering

Conceptual Insights

Perovskite ($CH_3NH_3PbI_3$) has recently become the "star" in the field of thin-film solar cell in the past two years. High power conversion efficiency and low material cost are two most fascinating advantages when utilizing this unique kind of organic-inorganic hybrid materials as photovoltaic absorbers. For the first time, this work demonstrates that perovskite absorber as wide bandgap material can be integrated into tandem solar design with other existing solar cell technology. Our work will study the design of tandem solar cell using perovskite absorber as building block, demonstrate the feasibility as well as the practical improvement in the performance, and hopefully convince the other solar cell technologies (e.g. silicon, CIGS, and III-V) to integrate perovskite materials into their tandem solar cell design for practical applications and better performances.

Perovskite/Polymer Monolithic Hybrid Tandem Solar Cell Utilizing Low-temperature, Full Solution Process

*Chun-Chao Chen, Sang-Hoon Bae, Wei-Hsuan Chang, Ziruo Hong, Gang Li, Qi Chen, Huanping Zhou, Yang Yang**

Departments of Materials Science & Engineering, University of California, Los Angeles, Los Angeles, California 90095, United States
*Corresponding Author: yangy@ucla.edu (Y. Y.)

Keywords: perovskite, polymer, solar cell, hybrid tandem solar cell, solvent wash, additive.

Abstracts: In current study, a monolithic integration of perovskite and polymer subcells in tandem structure is realized through full solution process. The wide bandgap perovskite absorber ($CH_3NH_3PbI_3$) is processed via one-step deposition employing the additive-assisted solvent wash method. Especially, small molecule additive, BmPyPhB, is added into precursor solution to improve the uniformity of initial nucleation process of crystal by providing the heterogeneous nucleation sites throughout the space. Next, the solvent wash method is employed to induce the fast crystallization of uniform and well-defined grains in the absorber layer as well as to reduce the requirement for thermal annealing. Thus highest power conversion efficiency (PCE) of 9.1% is obtained for single junction, planar-structured $CH_3NH_3PbI_3$ solar cell. For polymer absorber, a new IR-sensitive block copolymer, PBSeDTEG8, with photosensitive up to 950 nm is utilized to broaden the photoresponse of the tandem solar cell. More importantly, this polymer:PCBM blend exhibits improved thermal stability, which can endure thermal annealing while fabricating perovskite subcell. Subsequently, the hybrid tandem solar cells based on perovskite/polymer subcells achieves the highest efficiency of 10.2 %.

1. Introduction

Solar cell technology has been expected to be the most effective method in producing clean energy at low cost and minimum pollution. During the past two years, perovskite photovoltaic (PVSK-PV) have drawn intense attention due to its advantages such as high efficiency, mechanical flexibility, and simple fabrication method by solution coating.[1-5] Current progress in the power-conversion efficiency (PCE) of PVSK-PV has overcame the 19% PCE barrier, making PVSK-PV greatly attractive as next-generation, low-cost, and highly efficient photovoltaic (PV) candidate for solar energy harvesting.[6] Given that pursuing high efficiency is always the core task for photovoltaic device, one constrain is often found in perovskite sensitizer due to the weak light-harvesting capability in long wavelength region.[7] In the prototypical perovskite material, $CH_3NH_3PbI_3$, the sensitizer with fixed energy bandgap of 1.52 eV can only absorb photon energy up to 800 nm leaving more than half of the solar energy unharnessed.[8] Tandem solar cell consisting of two single-junction units stacked vertically in series connection is an effective approach to extend the photo-response of solar cell by utilizing absorbers with differentiated absorption spectra.[9, 10] Nevertheless, perovskite materials with bandgap smaller than 1.3 eV is still under development with limited success, the desirable absorber arrangement for tandem structure will require a non-perovskite based absorber with similar solution-process capability.[11-15] Polymer solar cell (PSC) emphasizing on the solution based fabrication has device architecture sharing similar interlayers (ex. metal oxide) as that of PVSK-PV.[16] Currently, PSC based on DPP main-chain structure has been reported with excellent near-IR photosensitivity up to 950 nm and a photocurrent output up to 17 mA/cm^2.[2, 17, 18] Based on the complementary absorption of perovskite and near-IR polymer absorbers, a hybrid perovskite/polymer tandem solar cell can be demonstrated to harness the full spectrum of solar energy thus a performance improvement can be expected.

In the few recently developed device structures for perovskite solar cell, the planar device architecture based on PEDOT:PSS and PCBM has been given great attention due the simple and low-temperature processing advantages.[19, 20] However, the performance of $CH_3NH_3PbI_3$-based sensitizer in planar structure

still remains unstable and inefficient. Without the mesoporous metal oxide (ex. TiO_2 and ZnO) as scaffold to support the growth of fine-size grain domain, the uncontrolled crystallization rate of precursor-intermediate phase (CH_3NH_3I-PbI_2) upon one-step spin-coating usually results in unfavorable perovskite morphology consist of numerous void and gap.[21] The resulting performance often suffers from the large leakage current caused by rough surface and poor interfacial contact, therefore, is far less than 15% PCE.[22, 23] Currently, Graztel *et al.* has shown that via vacuum evaporation method and modified interfacial contact a smooth morphology and improved PCE of 12% can be achieved for $CH_3NH_3PbI_3$-based sensitizer in planar structure.[19] However, there is still a lack of understanding on how to control the morphology of $CH_3NH_3PbI_3$ via one-step solution method, more importantly, how to minimize the thermal treatment required by perovskite phase formation. Here, we demonstrated a method utilizing additive-assisted solvent wash technique during spin-coating to enhance nucleation process and at the same time expedite the crystallization process of the intermediate phase (CH_3NH_3I-PbI_2), which ultimately gives us the favorable morphology for the perovskite phase ($CH_3NH_3PbI_3$). As the result, with demonstrated method the required thermal treatment can be reduced to 100 °C/5 min, making it compatible with polymer solar cell processing.

2. Morphological control of $CH_3NH_3PbI_3$

Previously, we have demonstrated a low-temperature method to process the perovskite absorber of $CH_3NH_3PbI_{3-x}Cl_x$.[24] During the formation of $CH_3NH_3PbI_{3-x}Cl_x$ from precursor phase to crystallite phase, it has been found to generate a by-product of CH_3NH_3Cl, which could be removed along the thermal treatment.[25] Nevertheless, the perovskite solar cells using $CH_3NH_3PbI_{3-x}Cl_x$ often requires a prolonged thermal treatment up to 2 hour at 90 or 100 °C to completely remove this by-product or convert it to $CH_3NH_3PbCl_3$.[26] Considering that the optimized morphology of polymer solar cell would degrade under extended heating,[27] the approach of $CH_3NH_3PbI_{3-x}Cl_x$ may not be suitable for the perovskite/polymer tandem structure here. On the other hand, the approach using $CH_3NH_3PbI_3$ as perovskite absorber may be

a solution to our concern. In order to obtain the desirable morphology and minimize the requirement of thermal treatment for $CH_3NH_3PbI_3$, the crystallization process of $CH_3NH_3PbI_3$ is explored in details.

Figure 1 provides the illustrations describing the crystallite growth of perovskite film in one-step coating process under different treatments. When solvent starts to evaporate during spin-coating, CH_3NH_3I-PbI_2 slowly precipitates out and form crystallite. Owing to the fact that planar structure lacks the metal oxide scaffold to support the crystallite growth, the morphology of perovskite tends to be controlled by the limited nucleation sites. When there is no extra treatment being provided to $CH_3NH_3PbI_3$, the crystallite growth often ends up in one-directional growing accompanying with large voids (Figure 1a). This first method without any modification is hereafter known as "non-modified method".

One simple way to solve this problem is through manipulate the rate of crystallite growth during spin-coating. Figures 1b and 1c demonstrate two methods of incorporating an extra step of solvent wash during the spin-coating to induce an instant crystallization of intermediate phase (CH_3NH_3I-PbI_2) and thus the surface coverage of the precursor film can be maximized. Here, the role of nonpolar solvent can be described as morphological catalyst. Seok et tal., have found that during the spin-coating process the dropping of non-polar solvent, such as toluene, can immediate reduce the original solvent content in precursor film and thus force crystallites to precipitate at instant.[28] The resulting film morphology typically has more uniform grain domain and improved surface coverage (Figure 1b). This second method is hereafter known as "solvent wash method".

Here, we introduce a third method modifying second method in order to improve its reproducibility and, at the same time, further eliminate the formation of small voids. In the original solvent wash method, it is found that toluene has to be dropped after certain duration of time during spin coating (e.g. 6 seconds). Within these 6 seconds, the nucleation of precursor-intermediate phase gets initiated and small crystallites begin to precipitate out. We proposed that the addition of small molecules, 1,3-Bis[3,5-di(pyridin-3-yl)phenyl]benzene (BmPyPhB), can enhance the initial nucleation process by providing heterogeneous

nucleation sites for precursor species to nucleate throughout the space. Thus, with numerous nucleates uniformly distributed in the film, the resulting precursor crystallites grew out of this setup are expected to be even more compact and void-free (Figure 1c), compared to the original solvent wash method (Figure 1b). We hereafter described this third method as "additive-assisted solvent wash method".

Figure 2 shows the AFM and SEM images corresponding to non-modified, solvent wash, and additive-assisted solvent wash perovskite thin film on PEDOT:PSS prior to the annealing treatment. From Figure 2a to 2c, AFM height images are presented, whereas from Figure 2d to 2f, the corresponding SEM images are given as well. Starting with Figure 2a and 2d, the non-modified $CH_3NH_3PbI_3$ via one-step deposition process is characterized. The morphology of given perovskite film has large roughness and low surface coverage. Moreover, there is a clear indication of needle-like crystallite, meaning that the crystal growth is mainly based on one-dimensional (1D) direction.[29] We suspect that such unfavorable morphology is mainly due to the lack of nucleation sites, which promotes formation of large crystallite, and slow crystal growth that allows nanocrystals growing into nano-needles.

From Figures 2b and 2e, solvent washed $CH_3NH_3PbI_3$ films via one-step deposition method are characterized. From AFM height image, the surface roughness of perovskite is greatly reduced making it free of large voids that is previously found in non-modified samples. When the nonpolar solvent (e.g. toluene) is applied onto the precursor film during spin-coating, the precursor species that are not soluble in toluene are force to crystallize and precipitate out right away. Therefore, the crystal growth is accelerated and finished right after solvent wash. Consequently, no prolonged heating is required since perovskite crystallite is already formed mostly. Furthermore, the absence of needle-like morphology also indicates that crystal growth is not confined in 1D anymore. From SEM image, the surface coverage is greatly improved; however, there are still small voids throughout the film. From Figure 2c and 2f, additive-assisted solvent washed $CH_3NH_3PbI_3$ via one-step deposition method is characterized. The AMF image indicates that the perovskite film is further planarized with adding BmPyPhB into precursor formulation. The grain size is smaller and more compact compared to original solvent wash method,

which can be ascribed to the increase of heterogeneous nucleation sites provided by BmPyPhB during crystal growth. Most importantly, from SEM image the number and the size of voids are further reduced, making this method even more suitable for solution based device fabrication at low temperature.

Figure 3a and 3b show the device structure and energy level diagram for planar-structured single junction perovskite solar cell. The photo-current density and voltage curve (*J-V*) for perovskite solar cell in planar single junction is given in Figure 3c and 3d. In Figure 3c, the perovskite planar junction is prepared by 3 different film growth methods introduced in Figure 1, e.g. non-modified, solvent wash, and additive-assisted solvent wash methods. The summary of performance parameters and thickness variations listed in Table 1. From Figure 2c, the The open-circuit voltage (V_{OC}) of the non-modified samples shows a major reduction compared to the other two processing conditions, which can be ascribed to the possibly non-continuous film morphology along with increased charge recombination. The poor fill factor (FF) also indicates that the charge transport is obstructed by compromised interfacial contacts with electrodes due to limited surface coverage. As the result, an unfavorable morphology obtained from non-modified precursor solution make the PCE of devices only as efficient as 4.7%.

On the other hand, the solvent washed samples show a great improvement to both short-circuit current density (J_{SC}) and FF, resulting in 7.2% PCE. Since both J_{SC} and FF is directly related to the charge collection capability, it is reasonable to believe that morphology of perovskite film after solvent wash becomes more favorable for device fabrication. Last, another 10% efficiency improvement for reaching 7.9% PCE is observed in the additive-assisted solvent washed samples, which we mainly ascribed to the effect of adding in small molecule additive and changing the nucleation process and final morphology. Concluding from above, the effectiveness of using solvent wash method as morphology modifier for perovskite has been validated through photovoltaic performance as shown above. The incorporation of BmPyPhB as additive in solution processing to further enhance the performance also supports our claim that small molecule additive inside precursor solution can be an another effective way to control morphology.

In Figure 3d, a series of three different annealing temperatures for a short duration of time (e.g. 5 minutes) is used to convert the precursor film from intermediate phase to perovskite phase based on additive-assisted solvent wash method. By increasing the temperature from 80 °C to 100 °C, the resulting device performance can be further improved from 7.9% to 9.1% PCE. Although the most efficient devices still are the ones baked at 100 °C, the samples processed from 80 °C can maintain up to 86% of the best efficiency achieved by the ones from 100 °C. Thus, this observation specifies a week dependence of device performance on the annealing temperature which can be mainly attributed to well crystallized perovskite phase induced by both solvent wash and small molecule additive methods prior to the annealing treatment. Therefore, no prolonged and high temperature annealing treatment is required for achieving optimized morphology for perovskite thin film.

3. Perovskite/Polymer Hybrid Tandem Solar Cell

Figure 4a demonstrates a device design for realizing the highly efficient hybrid tandem solar cell composed of perovskite and polymer absorbers. Due to the high absorption coefficient ($1x10^5$ 1/cm) of perovskite $CH_3NH_3PbI_3$ as compared to polymer ($6x10^4$ 1/cm),[30] we placed IR-polymers and fullerene derivatives as the bottom subcell absorbers in tandem devices to catch the incident light first, while the perovskite $CH_3NH_3PbI_3$ as top subcell absorbers can harness the remaining photons. Such arrangement of absorbers in tandem intends to balance the photocurrent generation from subcells and have a matched current density for maximizing the overall device performance. In Figure 4b, the photon absorption profile for each subcells in tandem are provided with calculated short-circuit current (J_{SC}). The optimal thickness adjustments for each subcells are found around 90-105 nm for polymer in the bottom subcell and 180-190 nm for perovskite in the top subcell.

Figure 4c provides the band diagram of complete hybrid tandem solar cell. In between the two subcells, the recombination layers are presented to function as electrical connection and to facilitate efficient charge recombination. Here, we presented a design of recombination layers based on metal oxide,

PEDOT:PSS, and conjugated polyelectrolyte made of poly [(9,9-bis(3'-(N,N-dimethylamino)propyl)-2,7-fluorene)-alt-2,7-(9,9–dioctylfluorene)] (PFN) all processed from solution method. Particularly for perovskite subcell, double electron and hole interlayers are introduced. PCBM with LUMO of 4.2 eV and PFN with surface dipole are used as electron transporting and hole blocking layers, respectively, to efficiently draw electrons out from perovskite absorbers and minimize interfacial recombination.[31] Similarly, double hole transporting layers can also realized here using PEDOT:PSS PH500 and AI 4083 as hole transporting and electron blocking layers, respectively.[10] AI 4083 with deeper work function (5.0 eV) and higher resistivity (100 ohm/square) can block electron more efficiently than PH500.

Besides the arrangement of absorbers and the design of recombination layers, the processing compatibility between perovskite and polymer presents another great challenge in demonstrating successful hybrid tandem solar cell. Particularly for polymer absorbers used in the bottom subcell, thermal stability is required in order to survive the thermal treatment (100 °C for 5 min) during the process forming perovskite phase of $CH_3NH_3PbI_3$. Here, we presented an alternation of popular narrow-bandgap polymer, PBDTT-SeDPP,[32] in the form of block copolymer, namely PBSeDTEG8. The chemical structures of PBSeDTEG8 absorbers used in the bottom subcells are shown in Figure 4d. Here, we found that PBSeDTEG8:PCBM photoactive layer can be processed without additive (such as DIO, CN) and still reach its optimal performance. This can be ascribed to its triethylene glycol side chain which can reinforce the stacking order of polymer chain thus maintaining a stable photovoltaic performance at elevated temperature.[33] From Table 1, PBSeDTEG8:PCBM single junction solar cell at pristine state without annealing can achieve 7.0% PCE. When annealed at 100 °C for 5 min, there is a slight drop in performance but still keeps at 6.6% PCE.

Next, we examine the photovoltaic performance of hybrid tandem solar cell composed of perovskite and polymer absorbers. Here, two different top electrodes are compared to identify the improvement resulted from the use of PFN as electrode interlayer. In Figure 5a, the result of *J-V* curses shows that with reflective Al (Al-based) electrode and a thick layer of perovskite (180 nm) as back subcell the hybrid

tandem solar cell can attain highest PCE = 9.13% for V_{OC} = 1.51 V, J_{SC} = 9.91 mA/cm^2, FF = 0.61. The V_{OC} of hybrid tandem solar cell is close to the sum of V_{OC} of perovskite (0.92 V) and polymer (0.66 V) subcells owing to the efficient recombination at interconnecting layers and negligible voltage loss for aligning the Fermi level between subcells. Furthermore, a modification of top electrode with PFN (PFN-based) is also demonstrated. In this setup, a thin layer of PFN is inserted between PCBM and Al electrode to improve the electron injection to electrode. The resulting performance shows that V_{OC} = 1.52 V, J_{SC} = 10.05 mA/cm^2, FF = 0.67, and a PCE = 10.23 %. The photocurrent density of PFN-based top electrode hybrid tandem solar cell is higher than that of Al-based top electrode hybrid tandem solar cell owing to PFN as dipole layer can efficiently lower the injection barrier for electron and block hole at the same time thus interfacial recombination is reduced. With the results obtained, we have successfully demonstrated monolithic hybrid tandem solar cell composed of perovskite and polymer absorbers by the full solution fabrication.

Furthermore, we took the EQE measurement for the PFN-based optimized tandem solar cells. The EQE measurement for the each subcell is provided in Figure 5b. To obtain accurate EQE results, one subcell is selectively turned on by monochromatic light bias while another subcell is taking the measurement.[34] The integrated current density from EQE is 9.9 mA/cm^2 for the bottom polymer subcell and 9.85 mA/cm^2 for the top subcell which are in a good agreement with both J-V characteristics and optical simulations. The reference EQE for single junction perovskite and polymer solar cells are provided in the same figure. Moreover, the *J-V* characteristics of single junction cells measured under the influence of optical interference similar to that experienced by the subcells in hybrid tandem structure are also provided in the supporting information. The results of J_{SC} are in a good agreement with calculated J_{SC} from EQE measurement here. These results suggest that our design of recombination layers have provided an optimized connection between the two subcells with least optical or electrical losses.

4. Conclusion

In conclusion, we have demonstrated the efficient hybrid tandem solar cells by integrating perovskite and polymer: fullerene as subcell absorbers. For perovskite, $CH_3NH_3PbI_3$ with photosensitivity up to 800 nm is utilized. To further improve morphology of perovskite and reduce the requirement of thermal treatment, solvent wash method is applied to control the crystal growth process along with small molecule additive, BmPyPhB, as source of heterogeneous nucleation sites to provide a continuous and dense morphology without large voids. With a fine morphology, $CH_3NH_3PbI_3$ single junction cell can attain 9.1% PCE using very mild thermal treatment of 100 °C for 5 minutes. In terms of recombination layers, double hole and double electron transporting layers are applied. More importantly, all these interlayers are solution processable thus maintain the orthogonal processing advantages for hybrid tandem solar cells.

Last, we introduced a new IR-polymer, PBSeDTEG8 with excellent thermal tolerance as the bottom subcell in our tandem devices. The hybrid tandem under this design can achieve an optimal efficiency of 9.13% which is greater than both of perovskite and polymer single junction cells used in our study. To further improve the contact with Al electrode, PFN as interfacial dipole layer is applied prior to the top electrode deposition. Device performance shows a promising improvement with higher FF and greater efficiency of 10.23%. In summary, the developments presented here have provided guidelines for designing effective tandem devices from solution-processed organic polymer materials and inorganic hybrid perovskite materials. Our work suggests a promising future for solution-based hybrid tandem solar cells using perovskite as building block. We expect that the PCE of this perovskite/polymer hybrid tandem system could reach 15% or above when new IR polymer with 10~12% PCE in single junction is realized and incorporated.

5. Experimental Section

Single Junction Solar Cell: The device architecture of the single junction cell is shown in Figure 2a. The devices were fabricated on ITO-coated glass substrates, with sheet resistance of 15 Ω/□. The pre-cleaned ITO substrates were treated with UV-ozone and then spin-coated with the PEDOT:PSS AI 4083 solution

by baking at 140 °C for 10 min in ambient air. The samples then transferred to a nitrogen-filled glove box for perovskite and polymer deposition. For polymer, the active layer of ~100 nm thickness was deposited by spin-coating PBSeDTEG8:$PC_{61}BM$ from 1:2 wt. ratio DCB solution. Ca/Al (20 nm/100 nm) electrode was thermally evaporated through shadow mask. For perovskite, the active layer of various thicknesses was deposited by spin-coating CH_3NH_3I:PbI_2 from 1:1 molar ratio DMF solution (42 wt.%) at 4000 rpm for 60 sec. For small molecule additive containing solution, there are 3% BmPyPhB with respect to the CH_3NH_3I:PbI_2. During the rotation after 6 sec, one drop of 20 μL toluene solvent is dropped on the sample to and there is an immediate color change from transparent to brownish.[28] Samples were annealed at 100 °C for 5 min.[29] The PCBM solution (2 wt.% in chlorobenzene) was spin-coated to form 50 nm layer.[35] Last, 100 nm of Al was thermally evaporated through shadow mask. The device area, as defined by the overlap between the ITO and Al electrodes, was 0.100 cm^2. The non-overlapping area is scratched out by razor blade to avoid the overestimation of J_{SC}.

Hybrid Tandem Solar Cell: The device architecture of the hybrid tandem cell is shown in Figure 4a. The tandem devices were fabricated on ITO-coated glass substrates, with sheet resistance of 15 Ω/□. First, the procedure follows the fabrication of single junction solar for polymer, without depositing the electrode. Then, inside the glovebox the interconnecting layers (ICL) used as recombination layers in tandem are formed. First, 5 nm thickness surface dipole layer was spin-coated from 0.02 wt.% PFN solution in methanol.[10] Next ICL of 30 nm thickness was deposited by spin-coating TiO_2 nanoparticle precursor solution from 0.2 wt.% ethanol solution.[17] Samples were annealed at 100 °C for 2 min. The PEDOT:PSS PH500 was spin-coated to form 60 nm layer, followed by 100 °C for 1 min. Similarly, the PEDOT:PSS AI 4083 was spin-coated to form 30 nm layer, followed by 100 °C for 1 min. The second active layer was spin-coated at 4000 r.p.m. for 60 s from CH_3NH_3I:PbI_2 (1:1 molar ratio) with 3% BmPyPhB in DMF solution (29 wt.%). Samples were solvent washed with toluene during spin-coating and annealed at 100 °C for 5 min. Last, 5 nm of PFN was deposited from same methanol solution. Finally, to complete the solar cell device, 100 nm of aluminum as the anode were thermally evaporated through a

shadow mask. The device area, as defined by the overlap between the ITO and Al electrodes, was 0.100 cm^2. The non-overlapping area is scratched out by razor blade to avoid the overestimation of J_{SC}.

Solar cell device measurement: The device layout is provided in the supporting information to show how the actual tandem devices were measured. The current density-voltage (*J-V*) characteristic curve of solar cells were measured with a 0.1 cm^2 shadow mask using a Keithley 2400 source-meter under a simulated AM1.5G solar illumination from a Newport solar simulator setup. A KG-5 filter silicon photodiode was used to calibrate the light intensity to 1 sun (100 mW/cm^2). To avoid overestimating photocurrent, each device was isolated completely by scratching the surrounding films around the device.[9] External quantum efficiencies (EQEs) were measured using an Enlitech QE-R spectral response measurement system. A SRC-2020 solar reference cell was used to calibrate the spectrum of EQE measurement. AFM and SEM measurements were performed at Nano & Pico Characterization Lab at California Nano Systems Institute and at Nanolab, respectively. The PL photons were counted by Picoharp 300 after pre-amplification by PAM102.

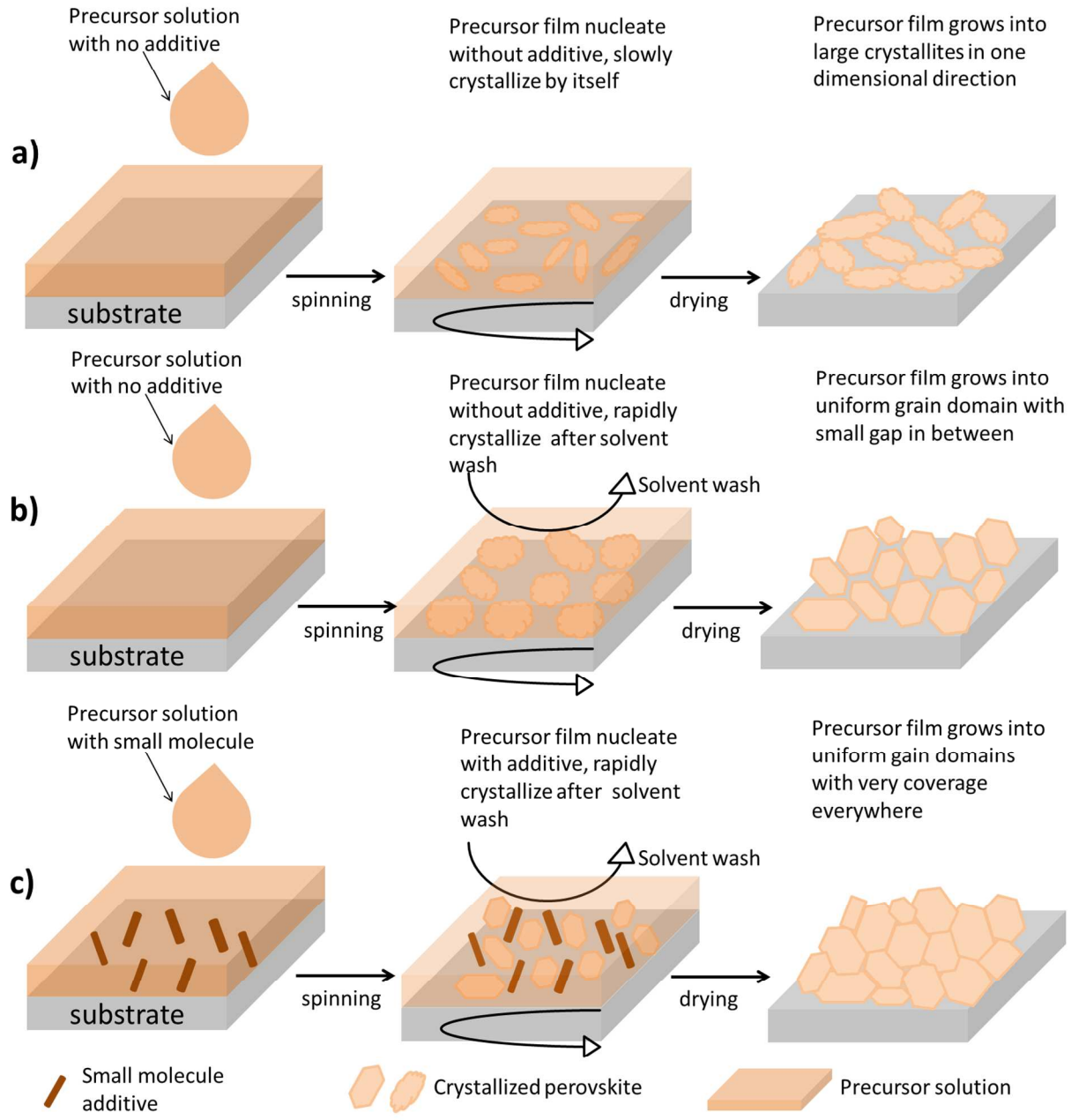

Fig.1 (a) Non-modified procedure for preparing the perovskite film without solvent wash and additive; (b) Solvent wash procedure for preparing the perovskite film; and (c) Additive-assisted solvent wash procedure for preparing the perovskite film.

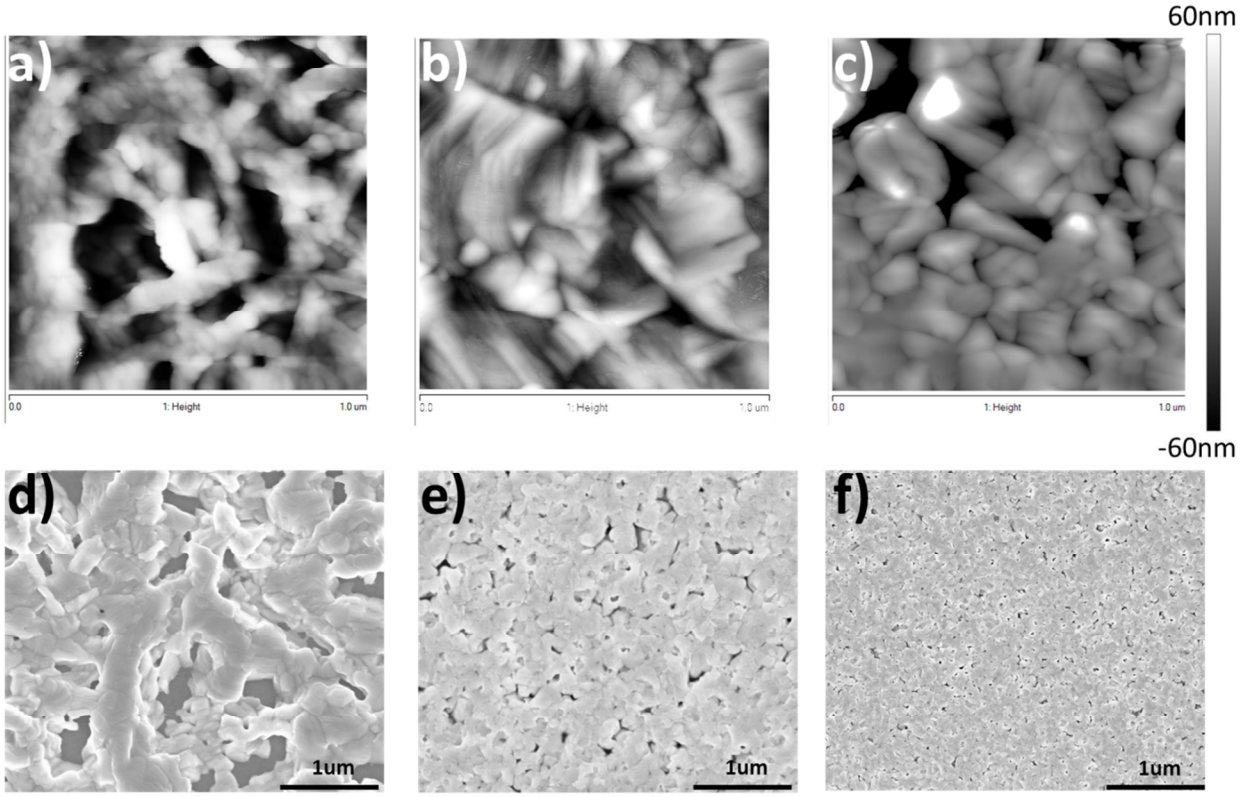

Fig.2 AFM topography of the perovskite film prior to thermal annealing processed from (a) non-modified, (b) solvent wash, and (c) additive-assisted solvent wash; similarly, SEM topography of the perovskite film post to thermal annealing processed from (d) non-modified, (e) solvent wash, and (f) additive-assisted solvent wash. The size of the AFM images is 1×1 μm^2. The scale bar for SEM images is 1 μm.

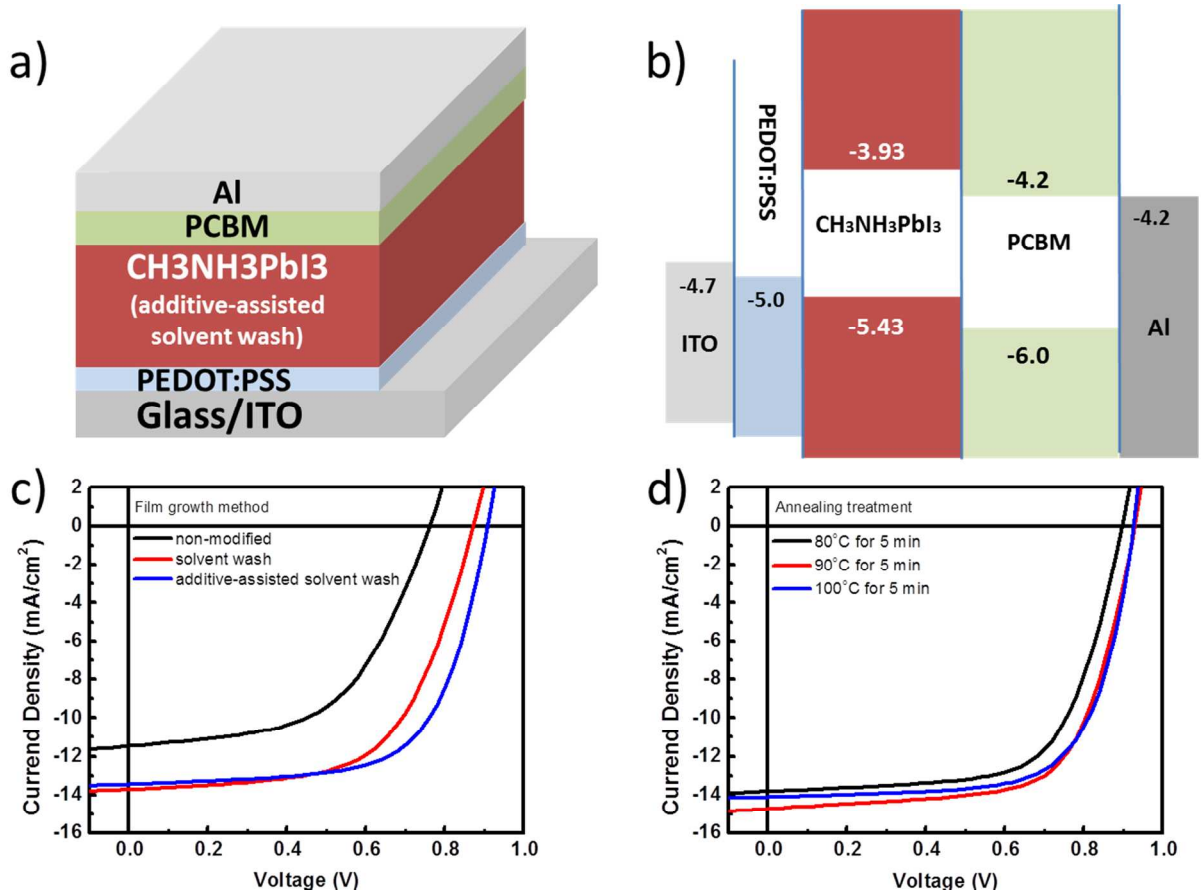

Fig.3 (a) Device architecture of the planar structure perovskite solar cell (glass/ITO/PEDOT:PSS/perovskite layer/PCBM/Al); (b) Proposed energy level landscape for perovskite solar cell; (c) *J–V* curves for a single junction cell processed via different methods; (d) *J–V* curves for a single junction cell processed via different annealing temperatures.

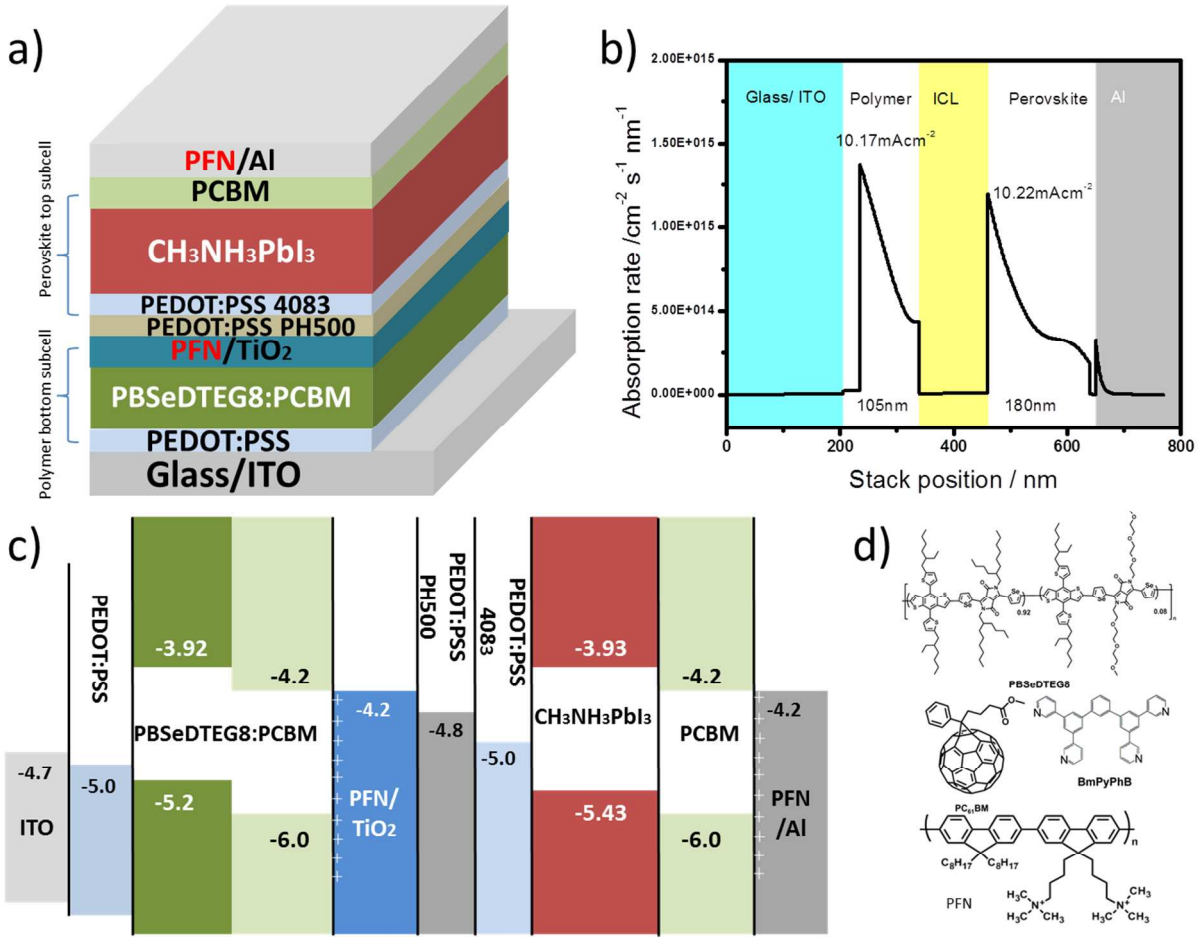

Fig.4 (a) Device architecture of the hybrid tandem solar cell composed of perovskite and polymer absorbers; (b) Photon absorption rate profile for each subcells inside hybrid tandem soalr cell; (c) Proposed energy level landscape for hybrid tandem solar cell; (d) Chemical structures of PBSeDTEG8, PCBM, BmPyPhB, and PFN.

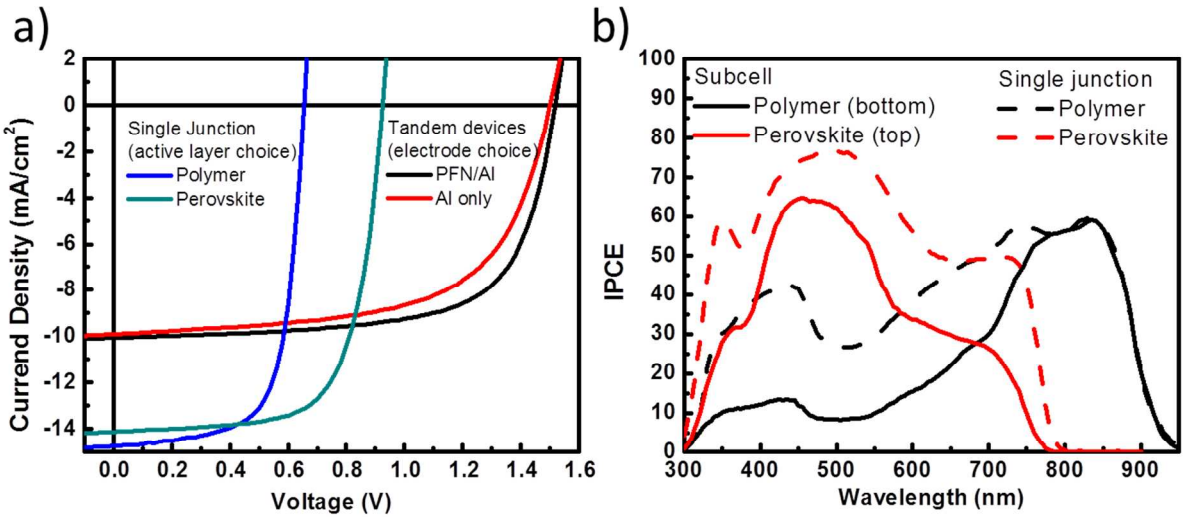

Fig.5 (a) *J-V* curves of hybrid tandem device made using different cathode choice and of perovskite and polymer absorbers in single junction setup; (b) External quantum efficiency of the perovskite and polymer subcells measured in the hybrid tandem device (solid lines) and of single junction reference devices made using same thickness perovskite and polymer layers (dash lines).

Table 1: Photovoltaic performance of perovskite single junction solar cells, polymer single junction solar cells, and hybrid tandem solar cells

$CH_3NH_3PbI_3$ single junction				
Film growth method	V_{OC} (V)	J_{SC} (mA/cm^2)	FF	PCE (%)
Non-modified	0.76	11.5	0.54	4.72
Solvent wash	0.88	13.8	0.60	7.28
Additive-assisted solvent wash	0.90	13.4	0.66	7.95
Annealing treatment	V_{OC} (V)	J_{SC} (mA/cm^2)	FF	PCE (%)
80 °C for 5 min	0.90	13.7	0.65	8.01
90 °C for 5 min	0.92	14.6	0.67	8.99
100 °C for 5 min	0.92	14.1	0.70	9.08
PBSeDTEG8 single junction				
Annealing treatment	V_{OC} (V)	J_{SC} (mA/cm^2)	FF	PCE (%)
Non-annealed	0.67	15.2	0.69	7.03
100 °C for 5 min	0.66	14.7	0.68	6.62
Hybrid tandem junction				
Cathode choice	V_{OC} (V)	J_{SC} (mA/cm^2)	FF	PCE (%)
Al only	1.51	9.91	0.61	9.13
PFN/Al	1.52	10.05	0.67	10.23

Acknowledgment

This work was financially supported by the Air Force Office of Scientific Research (AFOSR, Grant No. FA9550-09-1-0610), National Science Foundation (NSF ECCS-1202231), and UCLA internal funds. We like to thank Mr. Wei-Hsuan Chang for synthesizing low band gap polymer and Dr. Huanping Zhou for synthesizing MAI. We also like to thank Dr. Zirou Hong, Dr. Gang Li, and Dr. Qi Chen for proof-reading the manuscript. Last, authors also like to thank Nano & Pico Characterization Lab at CNSI for AFM measurement and Enlitech Co., Ltd., for providing EQE measurement equipment. C.C.C. would like to thank NSF-funded IGERT: Clean Energy for Green Industry Fellowship (Grant DGE-0903720).

References

1. A. Kojima, K. Teshima, Y. Shirai and T. Miyasaka, *J. Am. Chem. Soc.* , 2009, **131**, 6050-6051.
2. M. M. Lee, J. Teuscher, T. Miyasaka, T. N. Murakami and H. J. Snaith, *Science*, 2012, **338**, 643-647.
3. J. Burschka, N. Pellet, S.-J. Moon, R. Humphry-Baker, P. Gao, M. K. Nazeeruddin and M. Grätzel, *Nature*, 2013, **499**, 316-319.
4. J. H. Heo, S. H. Im, J. H. Noh, T. N. Mandal, C.-S. Lim, J. A. Chang, Y. H. Lee, H.-j. Kim, A. Sarkar and M. K. Nazeeruddin, *Nat. Photonics* 2013, **7**, 486-491.
5. M. Liu, M. B. Johnston and H. J. Snaith, *Nature*, 2013, **501**, 395-398.
6. H. Zhou, Q. Chen, G. Li, S. Luo, T.-b. Song, H.-S. Duan, Z. Hong, J. You, Y. Liu and Y. Yang, *Science*, 2014, **345**, 542-546.
7. M. A. Green, A. Ho-Baillie and H. J. Snaith, *Nat. Photonics* 2014, **8**, 506-514.
8. J. H. Noh, S. H. Im, J. H. Heo, T. N. Mandal and S. I. Seok, *Nano Lett.* , 2013, **13**, 1764-1769.
9. C. C. Chen, W. H. Chang, K. Yoshimura, K. Ohya, J. You, J. Gao, Z. Hong and Y. Yang, *Adv. Mater.* , 2014, **26**, 5670-5677.
10. C.-C. Chen, L. Dou, J. Gao, W.-H. Chang, G. Li and Y. Yang, *Energy Environ. Sci.* , 2013, **6**, 2714-2720.
11. N. K. Noel, S. D. Stranks, A. Abate, C. Wehrenfennig, S. Guarnera, A. Haghighirad, A. Sadhanala, G. E. Eperon, S. K. Pathak and M. B. Johnston, *Energy Environ. Sci.* , 2014.
12. F. Hao, C. C. Stoumpos, D. H. Cao, R. P. Chang and M. G. Kanatzidis, *Nat. Photonics* 2014, **8**, 489–494.
13. M. H. Kumar, S. Dharani, W. L. Leong, P. P. Boix, R. R. Prabhakar, T. Baikie, C. Shi, H. Ding, R. Ramesh and M. Asta, *Adv. Mater.* , 2014.
14. F. Zuo, S. T. Williams, P. W. Liang, C. C. Chueh, C. Y. Liao and A. K. Y. Jen, *Adv. Mater.* , 2014.
15. F. Hao, C. C. Stoumpos, R. P. Chang and M. G. Kanatzidis, *J. Am. Chem. Soc.* , 2014, **136**, 8094–8099.
16. S. Chen, J. R. Manders, S.-W. Tsang and F. So, *J. Mater. Chem.* , 2012, **22**, 24202-24212.

17. C. C. Chen, L. Dou, R. Zhu, C. H. Chung, T. B. Song, Y. B. Zheng, S. Hawks, G. Li, P. S. Weiss and Y. Yang, *ACS Nano*, 2012, **6**, 7185-7190.
18. L. Dou, C.-C. Chen, K. Yoshimura, K. Ohya, W.-H. Chang, J. Gao, Y. Liu, E. Richard and Y. Yang, *Macromolecules*, 2013, **46**, 4734–4734.
19. O. Malinkiewicz, A. Yella, Y. H. Lee, G. M. Espallargas, M. Graetzel, M. K. Nazeeruddin and H. J. Bolink, *Nat. Photonics* 2014, **8**, 128-132.
20. P. Docampo, J. M. Ball, M. Darwich, G. E. Eperon and H. J. Snaith, *Nat. Commun.*, 2013, **4**, 2761.
21. E. Edri, S. Kirmayer, A. Henning, S. Mukhopadhyay, K. Gartsman, Y. Rosenwaks, G. Hodes and D. Cahen, *Nano Lett.* , 2014, **14**, 1000-1004.
22. Q. Wang, Y. Shao, Q. Dong, Z. Xiao, Y. Yuan and J. Huang, *Energy Environ. Sci.* , 2014.
23. Z. Xiao, C. Bi, Y. Shao, Q. Dong, Q. Wang, Y. Yuan, C. Wang, Y. Gao and J. Huang, *Energy Environ. Sci.* , 2014, **7**, 2619-2623.
24. J. You, Z. Hong, Y. Yang, Q. Chen, M. Cai, T.-B. Song, C.-C. Chen, S. Lu, Y. Liu and H. Zhou, 2014.
25. A. Dualeh, N. Tétreault, T. Moehl, P. Gao, M. K. Nazeeruddin and M. Grätzel, *Adv. Funct. Mater.* , 2014.
26. Y. Zhao and K. Zhu, *J. Phys. Chem. C*, 2014.
27. G. Griffini, J. D. Douglas, C. Piliego, T. W. Holcombe, S. Turri, J. M. Fréchet and J. L. Mynar, *Adv. Mater.* , 2011, **23**, 1660-1664.
28. N. J. Jeon, J. H. Noh, Y. C. Kim, W. S. Yang, S. Ryu and S. I. Seok, *Nat. Mater.* , 2014, **13**, 897–903.
29. M. Xiao, F. Huang, W. Huang, Y. Dkhissi, Y. Zhu, J. Etheridge, A. Gray-Weale, U. Bach, Y. B. Cheng and L. Spiccia, *Angew. Chem.*, 2014, **126**, 10056-10061.
30. J. Yan and B. R. Saunders, *RSC Advances*, 2014, **4**, 43286-43314.
31. H. Zhang, H. Azimi, Y. Hou, T. Ameri, T. Przybilla, E. Spiecker, M. Kraft, U. Scherf and C. J. Brabec, *Chem. Mater.* , 2014, **26**, 5190–5193.
32. L. Dou, W. H. Chang, J. Gao, C. C. Chen, J. You and Y. Yang, *Adv. Mater.* , 2013, **25**, 825-831.
33. W. H. Chang, J. Gao, L. Dou, C. C. Chen, Y. Liu and Y. Yang, *Adv. Energy Mater.*, 2014, **4**.
34. L. Dou, J. You, J. Yang, C.-C. Chen, Y. He, S. Murase, T. Moriarty, K. Emery, G. Li and Y. Yang, *Nat. Photonics* 2012, **6**, 180-185.
35. C. Zuo and L. Ding, *Nanoscale*, 2014, **6**, 9935-9938.

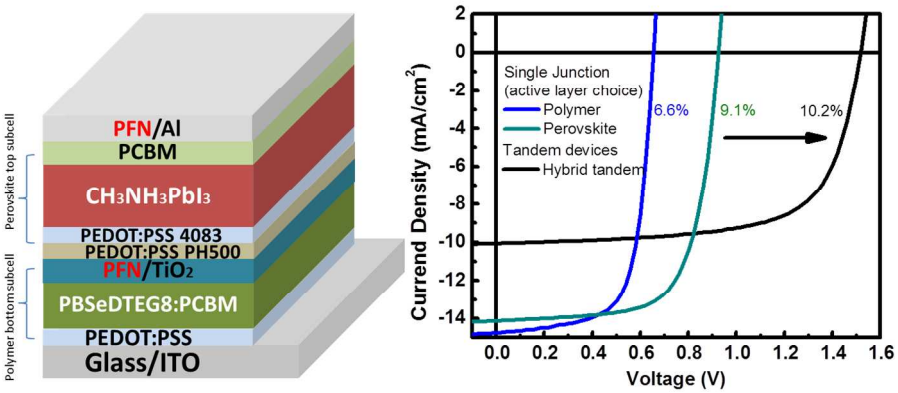

Graphical abstract